Journal of Defense Analytics and Logistics

Convexity of intercept time in short-range re-entry vehicle defence: how to optimally intercept a fast re-entry vehicle travelling in a lofted trajectory

Received 5 June 2025
Revised 26 February 2026
10 March 2026
Accepted 10 March 2026

Phuc Bao Uyen Nguyen
Centre for Operational Research and Analysis, Defence Research and Development Canada, Ottawa, Canada and Faculty of Engineering, University of Ottawa, Ottawa, Canada, and
Alexander Urquhart, Maude Amyot-Bourgeois and Brittany Astles
Centre for Operational Research and Analysis, Defence Research and Development Canada, Ottawa, Canada

Abstract

Purpose – The described anomaly allows an interceptor to intercept a threat that has superior speed. The results account for gravity and would not occur if the trajectories of the threat and the interceptor were modelled as simple straight lines. The algorithm could be tested experimentally. The article also provides a criteria for feasible intercepts in general at short ranges.

Design/methodology/approach – The derivation of the optimal intercept time with gravity is non-trivial and would be intractable using calculus. The optimization is done in the velocity phase space instead of the time of flight. In addition, the proof of the convexity of the intercept time is complex, requiring intricate arguments. We also make use of a dimensionless scaling technique that simplifies the derivation.

Findings – There are two main results that arise from the intercept time formula. First, there is a unique optimal delay in launching the interceptor to minimize total intercept time. Second, there is a feasible volume of approach that changes with time, where it is possible to intercept the RV. If the interceptor lies outside of this volume, then an intercept is not possible.

Research limitations/implications – The derivation is made assuming short-range missile defence scenarios and environmental conditions, such as air friction and tracking, are not modelled.

Practical implications – The algorithm allows a slow interceptor to intercept a fast threat. This allows, for example, a Patriot interceptor to intercept a hypersonic missile.

Social implications – This helps defence of assets against short-range missiles.

Originality/value – The derivation of the intercept time formula of an RV by a ballistic interceptor is not simple due to the non-linearity of the gravitational force. Adding to the complexity is the non-zero detonation range: an interceptor explodes when it reaches a certain non-zero range to the RV. The anomaly of the intercept time is unexpected, as the usual wisdom may be to launch the interceptor as soon as a threat is detected. This would be true if trajectories were straight lines (in the absence of gravity).

Keywords Gravity, Convex optimization, Scaling law, Missile defence, Short range missiles

Paper type Research article

Introduction

Ballistic trajectories are determined by the gravitational field as well as the initial conditions of the vehicle: the launch location and the launch velocity. At short ranges (relative to the Earth's radius), we can consider the Earth as flat and the gravitational force as a constant. We will focus

Journal of Defense Analytics and Logistics
Emerald Publishing Limited
e-ISSN: 2399-6447
p-ISSN: 2399-6439
DOI 10.1108/JDAL-06-2025-0015

on short-range problems in this article. Cases of intermediate and long-range ballistic missile defence are more complex and can be found, for example, in (Buontempo, 2015; Carnegie Endowment for International Peace, 2021; Weitz, 2013). This is also a high-level analysis that examines the physics of short-range ballistic missile defence – environmental conditions such as atmospheric parameters are not considered, nor are tactics and manoeuvres. Detailed models have been the subject of intensive research and examples may be found in Ann *et al*. (2020), Carpentier (2014) and Lui *et al*. (2023).

There are two possible trajectories for getting from the origin location A to the final location B: a depressed trajectory with a (low) launch angle less than 45^o and a lofted trajectory with a (high) launch angle of more than 45^o, as shown below.

Figure 1 shows several trajectories of re-entry vehicles (RVs). The RV assumes an initial speed equal to $MACH$ 5. There are two types of trajectories: the dashed lines correspond to the low-angle trajectories, while the solid lines correspond to the high-angle trajectories. We refer to the low-angle (high-angle) trajectories as the depressed (lofted) trajectories. The depressed trajectories have a maximal $z \leq 20\,km$ and the lofted trajectories have a maximal $z \geq 120\,km$, where z is the altitude of the RV. Here, the RV is launched from the ground $(z = 0)$, travels from right to left and aims for the defense location at the origin $(0, 0)$.

Lofted trajectories are advantageous for RVs as they force the defence's radars to scan a large volume of space, which reduces search capabilities (Glover and Hagan, 1971). In addition, a lofted trajectory reduces the risk of civilian casualties in the event of a mid-air interception, since such a trajectory is located high above the ground. For example, the North Korean Hwasong-17 and Hwasong-18 intercontinental RVs employ lofted trajectories (Lendon and Bae, 2023). In addition, the Iranian Emad missile, employed in the 2024 attacks on Israel, is known to exit and re-enter the atmosphere (Pleitgen, 2024). This implies a lofted trajectory. The presence of a lofted trajectory is confirmed based on footage obtained from the BBC (Spender, 2024). We re-sketch the original figure from the BBC and estimate an angle of 48^o, which necessitates a lofted trajectory (Figure 2).

In general, the mathematics of ballistic trajectories is complicated, but they can be determined using astrodynamics through Kepler and Gauss algorithms (Bate *et al*., 1971; Vallado, 1997). However, short-range ballistic trajectories are considerably simplified since they are quadratic functions of time. Yet, the intercept time formula of an RV by a ballistic interceptor is not simple due to the non-linearity of the gravitational force, even at short ranges.

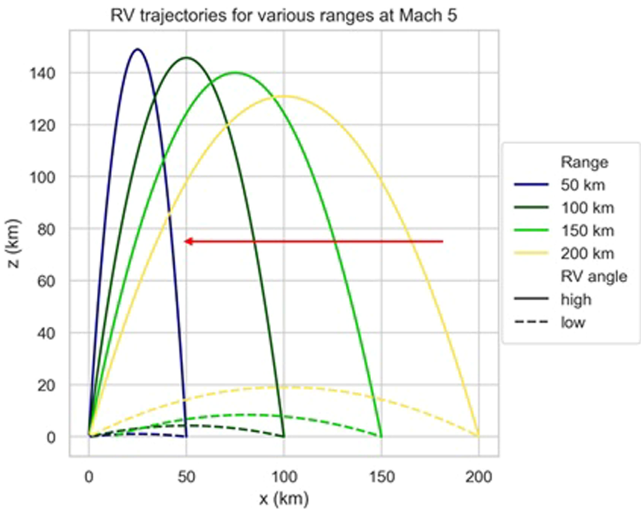

Figure 1. RV lofted (high) and depressed (low) trajectories

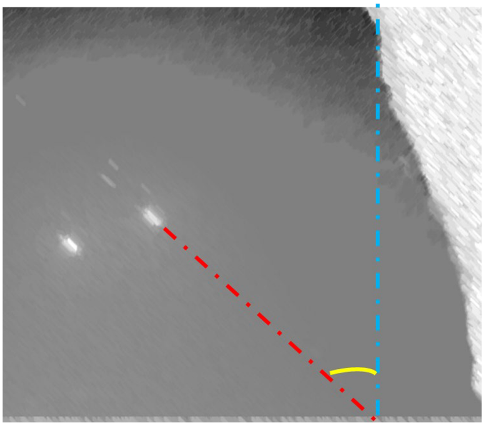

Figure 2. Lofted RV trajectory ($\mathbf{48^o}$) during Iranian attack against Israel

Adding to the complexity is the non-zero detonation range: an interceptor explodes when it reaches a certain non-zero range to the RV.

In this article, we derive the formula of the intercept time that accounts for the RV initial location, the RV initial velocity, the interceptor initial location, the interceptor launch delay time, the interceptor speed and the detonation range and gravity. We show through the convexity of the intercept time as a function of the interceptor launch delay time that if the RV's speed is greater than the interceptor's speed and if the RV's trajectory is lofted, then there is an optimal delay that minimizes the intercept time. We refer to this phenomenon as an anomaly in intercept time (Nguyen *et al*., 2022). Minimizing the intercept time affects intercept location, engagement opportunities and the probability of raid negation (Armstrong, 2014; Bourn, 2012; Cranford, 2004; Menq *et al*., 2007; Mury and Nguyen, 2007; Nguyen, 2014; Nguyen *et al*., 1997; Soland, 1987; Wilkening, 1999).

The article is organized as follows. First, we describe the scenarios. Second, we derive an analytical formula for the intercept time. Third, we derive the feasible volume of approach. Fourth, we show that there is an optimal launch delay to minimize the intercept time. Fifth, we show that there is only one minimal intercept time. Sixth, we interpret the results through examples. Finally, we provide a discussion and a conclusion.

Scenarios

We assume that the RV is like the Scud missiles deployed during the Gulf War by Iraq in 1990–1991 and the interceptor is like the Patriot missiles. Tables 1 and 2 show their characteristics (Wikipedia, 2022a, b). We also assume that the target location of the RV and the launch location of the interceptor are the same to illustrate the anomaly.

Table 1. Characteristics of the RV where MACH **1** is the speed of sound 0.343 km/s

Scud type	Speed (km/s)	Range (km) and location (Range, 0,0)
Scud A	1.7 (MACH 5)	180
Scud B		300
Scud C		600
Scud D		700

Table 2. Characteristics of the interceptor (MACH 6 is hypothetical)

Speed	MACH 2, 3, 4, 6*
Range (*km*)	50, 100, 150, 200
Detonation Range (*m*)	1, 2, 5

Intercept time

The intercept occurs when the interceptor reaches the detonation range from the RV. We can write the intercept equations as:

$$\begin{aligned} x_i^0 + v_x \cdot T &= x_m^0 + u_x \cdot T + x_\alpha \\ y_i^0 + v_y \cdot T &= y_m^0 + u_y \cdot T + y_\alpha \\ z_i^0 + v_z \cdot T - 1/2 \cdot g \cdot T^2 &= z_m^0 + u_z \cdot T - 1/2 \cdot g \cdot T^2 + z_\alpha \end{aligned} \tag{1}$$

Where

$$x_a^2 + y_a^2 + z_a^2 = a_a^2 \tag{2}$$

$T = t_{int}$ is measured from the time when the interceptor is launched; $\left(x_i^0 \quad y_i^0 \quad z_i^0 \right)$ is the location of the launch site of the interceptor; $\left(x_m^0 \quad y_m^0 \quad z_m^0 \right)$ is the location of the RV at the interceptor launch time (this is not necessarily the location of the launch site of the RV); $\left(x_\alpha \quad y_\alpha \quad z_\alpha \right)$ is the location of detonation on the sphere of radius α_0 (detonation range) measured from the location of the RV; $\vec{u}$ is the velocity of the RV at time t (it is not necessarily the velocity of the RV at its launch time) and it is known while v is the speed of the interceptor.

Even though gravity terms cancel in Equation (1), the intercept location $\vec{R}_{int}$ must include gravity since the vehicles are both subject to gravitational acceleration as seen below:

$$\vec{R}_{int} = \left(x_i^0 + v_x \cdot T \quad y_i^0 + v_y \cdot T \quad z_i^0 + v_z \cdot T - 1/2 \cdot g \cdot T^2 \right) \tag{3}$$

We aim to determine the direction of $\hat{v} = \left(cos\,\theta \cdot sin\,\varphi \quad sin\,\theta \cdot sin\,\varphi \quad cos\,\varphi \right)$ so that the intercept time is as short as possible. It is practically impossible to solve for the direction of $\hat{v}$ analytically from Equations (1) and even with the help of symbolic software such as Maple, Mathcad or Mathematica. That is, to minimize the intercept time as a function of (θ, φ) would involve solving a sixth-order polynomial with a few hundred terms once the derivative is radicalized (Nguyen and Nguyen, 1996). Therefore, this is a non-trivial mathematical problem.

Below, we derive a closed-form solution for the shortest intercept time that satisfies Equations (1) and (2) using geometry instead of calculus. Using Equation (1), we get:

$$\begin{aligned} x_\alpha &= \left(x_i^0 - x_m^0 \right) + \left(v_x - u_x \right) \cdot T \\ y_\alpha &= \left(y_i^0 - y_m^0 \right) + \left(v_y - u_y \right) \cdot T \\ z_\alpha &= \left(z_i^0 - z_m^0 \right) + \left(v_z - u_z \right) \cdot T \end{aligned} \tag{4}$$

Substituting Equation (4) into Equation (2), we get:

$$\frac{\alpha_0^2}{T^2} = \left[v_x - \left(u_x + \frac{x_m^0 - x_i^0}{T} \right) \right]^2 + \left[v_y - \left(u_y + \frac{y_m^0 - y_i^0}{T} \right) \right]^2 + \left[v_z - \left(u_z + \frac{z_m^0 - z_i^0}{T} \right) \right]^2 \tag{5}$$

Since we know the speed of the interceptor:

$$v^2 = v_x^2 + v_y^2 + v_z^2 \tag{6}$$

We observe that Equations (5) and (6) are now equations for spheres in the variables $(v_x \quad v_y \quad v_z)$. Each sphere has a different radius and a different centre. Equation (5) dictates that the first sphere has a radius equal to α_0/T and its centre is at $\left(u_x + \frac{x_m^0 - x_i^0}{T} \quad u_y + \frac{y_m^0 - y_i^0}{T} u_z + \frac{z_m^0 - z_i^0}{T}\right)$. Equation (6) dictates that the second sphere has a radius equal to v and its centre is at the origin $(0, 0, 0)$.

To have a common solution in $(v_x \quad v_y \quad v_z)$, the two spheres must intersect one another. If the spheres do not intersect, the $(v_x \quad v_y \quad v_z)$ solution of one sphere will not correspond to the $(v_x \quad v_y \quad v_z)$ solution of the other sphere. This means that the distance between the two spheres' centres is greater than or equal to the difference of their radii and less than or equal to the sum of their radii as shown in Figure 3. This can be expressed as:

$$\left(v - \frac{\alpha_0}{T}\right)^2 \leq \left(u_x + \frac{x_m^0 - x_i^0}{T}\right)^2 + \left(u_y + \frac{y_m^0 - y_i^0}{T}\right)^2 + \left(u_z + \frac{z_m^0 - z_i^0}{T}\right)^2 \leq \left(v + \frac{\alpha_0}{T}\right)^2 \tag{7}$$

We note that t is the only unknown in Equation (7). Nguyen and Nguyen (1996) determine the shortest intercept time t_{int} satisfying Equation (8):

$$T = t_{int} = \frac{\Delta r^0}{v} \cdot \left(\frac{-F + \sqrt{F^2 + (1 - \beta^2) \cdot (1 - \alpha^2)}}{1 - \beta^2}\right) \tag{8}$$

Where $\beta = \frac{u}{v}$, $\alpha = \frac{\alpha_0}{\Delta r^0}$, $cos(\theta^0) = \frac{\vec{u} \cdot \Delta \vec{r}_0}{u \cdot \Delta r_0}$, $\Delta \vec{r}^0 = (x_i^0 - x_m^0 \quad y_i^0 - y_m^0 \quad z_i^0 - z_m^0)$ and $F = \alpha + \beta \cdot cos(\theta^0)$.

t_{int} is measured from the launch time t of the interceptor. Hence, the total intercept time is given by $T \leftarrow t + T = t + t_{int}(t)$ measured from the time that the RV is launched. Based on this formula, we plot the total intercept time T as a function of $\chi = t/T_F$ (where T_F is the time of flight of the RV and $0 \leq \chi \leq 1$) in Figure 4. Four ranges are considered: the RV is initially $50, 100, 150\, and\, 200\, km$ away from the interceptor location. There are four scenarios (clockwise from top left):

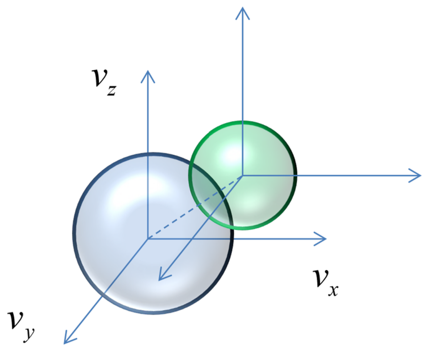

Figure 3. Intersecting spheres

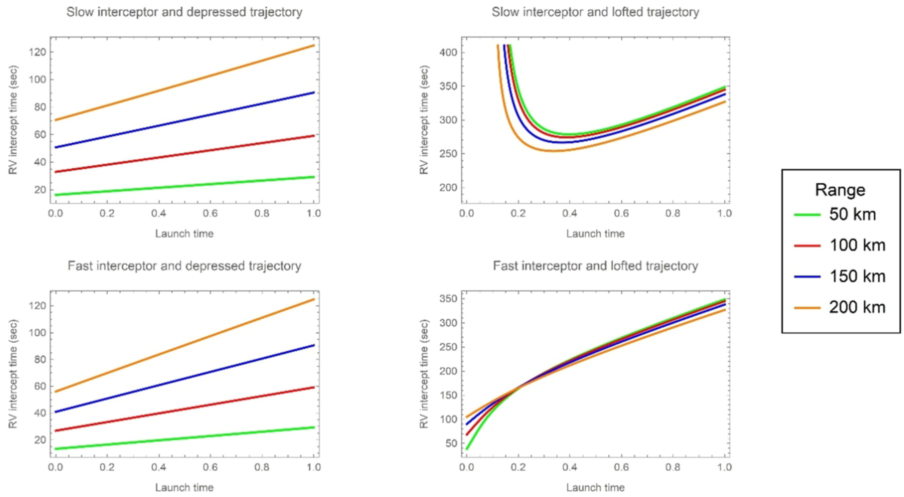

Figure 4. Four combinations of intercept

(1) Slow interceptor (interceptor's speed is less than RV's speed) and depressed RV's trajectory;

(2) Slow interceptor and lofted RV's trajectory;

(3) Fast interceptor (interceptor's speed is greater than RV's speed) and lofted RV's trajectory and

(4) Fast interceptor and depressed RV's trajectory.

We can see clearly the anomaly in Figure 4: there is a minimum in the total intercept time as a function of launch time (Figure 4, top right panel). This corresponds to the scenario where the interceptor's speed is less than the RV's speed and the RV's trajectory is lofted. In all the remaining scenarios, the total intercept time is monotonically increasing as a function of launch time.

In the following sections, we will examine carefully when and why the anomaly occurs.

Feasible volume of approach

In the formula for t_{int}, there is a radical (square root). If the argument of the radical is negative, then t_{int} is complex, which means that it is not physically possible to intercept the RV. Assuming that the RV is initially beyond the detonation range $(\alpha < 1)$ and knowing that $F^2 \geq 0$, this means that t_{int} can only be complex when $\beta = \frac{u(t)}{v} > 1$. Therefore, if the interceptor's speed is less than the RV's speed then it can happen that intercept is impossible.

Analysing the argument of the radical, we obtain a feasible volume of approach for the interceptor. That is, if the interceptor is slower than the RV, then to intercept the RV, the interceptor must initially be in the feasible volume of approach, as depicted below. In general, the interceptor's initial location must be in front of the RV's direction. The feasible volume of approach becomes larger with a non-zero detonation range. This feasible volume is a cone subtended by an angle θ_f (Figure 5):

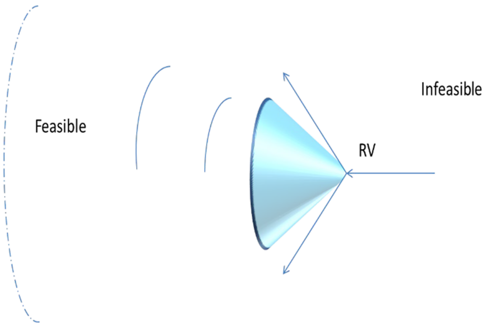

Figure 5. Feasible volume of approach

$$\theta_f = cos^{-1}\left(\frac{-\alpha + \sqrt{\left(\beta(t)^2 - 1\right)\cdot(1-\alpha^2)}}{\beta(t)}\right) \tag{9}$$

Knowing the feasible volume of approach tells us that if the RV's initial launch angle is too steep, then it is not possible for the interceptor to intercept the RV. However, if the defence waits for a certain time, the velocity of the RV will change as it turns towards its target and eventually the interceptor's location will be within the feasible volume of approach. This is shown in Figure 6 where the interceptor location is the black, hollow circle on the left-hand side and the RV's launch location is the red dot on the right-hand side of the horizontal line. Initially, the interceptor's location is outside of the angle subtended by the red lines (red feasible volume of approach); hence intercept is not possible. But at a later time, the RV has moved to the green dot, the interceptor's location is now inside of the angle subtended by the green lines (green feasible volume of approach); hence intercept is possible. The feasible volume of approach changes with time because the velocity vector and the location of the RV change with time due to gravity.

The simple argument of evolving a feasible volume of approach suggests why the interceptor should delay its launch time so that the intercept is optimal.

Existence of a minimal intercept time

The intercept time formula can be rewritten as follows:

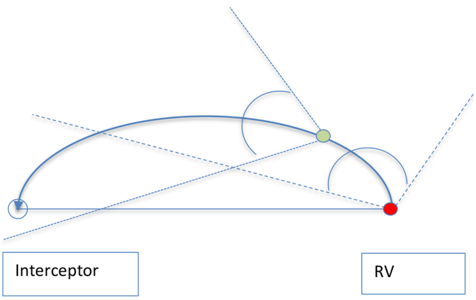

Figure 6. Evolving feasible volumes of approach (for illustration only, not drawn to scale)

$$t_{int} = \frac{-S + \sqrt{S^2 + D \cdot N}}{D} \tag{10}$$

S, D and N are defined as follows:

$$S = \alpha \cdot \gamma + (1 - \chi) \cdot \left(1 - tan^2(\theta) \cdot \chi + 2 \cdot tan^2(\theta) \cdot \chi^2\right)$$

$$D = \gamma - 1 - tan^2(\theta) \cdot (1 - 2 \cdot \chi)^2$$

$$N = (1 - \chi)^2 \cdot \left(1 + \tan^2(\theta) \cdot \chi^2\right) - \alpha^2$$

$$\chi = t / T_F$$

$$tan(\theta) = u_y / u_x$$

$$\gamma^2 = v^2 \cdot \frac{T_F^2}{R^2} = v^2 \Big/ \left(u^2 \cdot cos^2(\theta)\right)$$

$$\frac{v^2}{u^2} < 1$$

Where T_F is the time of flight of the RV and R is the horizontal range of the RV. It is convenient to analyze the intercept time in the dimensionless parameter χ, which is normalized by the time of flight. If the results are true in χ then they are true for all times of flight.

Note that Equation (10) contains a removable singularity when $D = 0$ (Nguyen and Nguyen, 1996):

$$D \cdot {t_{int}}^2 + 2 \cdot S \cdot t_{int} - N = 0 \tag{11}$$

So, if $D = 0$, we get:

$$t_{int} = \frac{1}{2} \cdot \frac{N}{S} \tag{12}$$

We will assume that $D \neq 0$. The special case where $D = 0$ will be explained later. We will show that the derivative of the total intercept time, T' (where $/T_F = \chi + t_{int}(\chi)$), is negative for a value of χ on the left-hand side and is positive for a value on the right-hand side (Figure 4, top right panel). For conciseness, we refer to T/T_F as T since T_F is a constant parameter in the problem. Since T' is a continuous function, there will be a χ such that $T'(\chi) = 0$ which corresponds to a minimum.

T is decreasing on the left-hand side.

Let $Z = S^2 + D \cdot N$, then:

$$T' = \frac{1}{D}\left(-S' + \frac{1}{2} \cdot \frac{Z'}{\sqrt{Z}}\right) - \frac{D'}{D^2} \cdot \left(-S + \sqrt{Z}\right) + 1 \tag{13}$$

$$\lim_{Z \to 0^+} T' \to \frac{1}{2 \cdot D} \cdot \frac{Z'}{\sqrt{Z}} \tag{14}$$

Note that $N \geq 0$ as it is proportional to the distance from the interceptor to the RV minus the detonation range and we assume that the RV is initially beyond the detonation range. Also, $S^2 \geq 0$ as S is real. So, if $Z \to 0^+$, this makes $D < 0$ since $Z = S^2 + D \cdot N$. This also means that the interceptor's speed is less than the RV speed at time χ. We claim that

$$\lim_{Z \to 0^+} T' \to \frac{1}{2 \cdot D} \cdot \frac{Z'}{\sqrt{Z}} = -\infty \tag{15}$$

That is, the total intercept time T is decreasing on the left-hand side if $\lim_{Z \to 0^+} Z' > 0$. We first assume that $\alpha = 0$ and solve for χ when $Z = 0$. There is a double root at $\chi = 1$ as well as two non-trivial roots:

$$\chi_{\pm} = \frac{-tan^2\,\theta \pm \sqrt{\gamma^2 \cdot tan^2\,\theta \cdot (1 - \gamma^2 + tan^2\,\theta)}}{tan^2\,\theta \cdot (\gamma^2 - 1)} \tag{16}$$

Case 1. $\mathbf{1 < \gamma <} \boldsymbol{tan}\,\theta$

It can be checked that: $0 < \chi_+ < 1$ and $\chi_- < 0$. So χ_+ corresponds to the left-hand side of the feasible launch time. In addition,

$$Z(\chi = 0) = \gamma^2 - tan^2\,\theta < 0$$

$$Z(\chi = 1) = 0$$

Since χ_+ is the only root strictly between zero and one, this means that Z must cross the zero value in an increasing way. Hence, $Z'(\chi_+) > 0$.

When $\alpha > 0$, we get:

$$Z(\chi = 0) = (\gamma + \alpha)^2 - tan^2\,\theta \cdot \left(1 - \alpha^2\right) < 0$$

$$Z_\alpha > 0$$

Where Z_α is the value of Z when the interceptor reaches the detonation range from the RV. That is, $N = 0$. An example of Z as a function of χ is shown in Figure 7. The red curve corresponds to $\alpha > 0$ ($\gamma = 7.187$, $tan\,\theta = -11.921$ and $\alpha = 0.3$) while the blue curve corresponds to $\alpha = 0$ ($\gamma = 1.682$ and $tan\,\theta = -2.619$). Note χ_+ moves to the left when $\alpha > 0$. This means that the interceptor can be launched earlier and still intercept the RV if given a non-zero detonation range.

Case 2. Other cases.

The proof is like Case 1.

T is increasing on the right-hand side.

We now show that $T' > 0$ as $\chi \to 1^-$. For simplicity, we write $\chi \to 1^-$ to refer to the case where the defense waits for the RV to reach the detonation range of its aimed destination. Technically, for small α, $\chi \sim 1 + \alpha \cdot cos\,\theta$ where $(cos\,\theta < 0)$. Note that $N = 0$ and $t_{int} = 0$ at $\chi \to 1^-$, as the RV has reached the weapon range. Therefore, differentiating Equation (11) and set $N, t_{int} = 0$ yields:

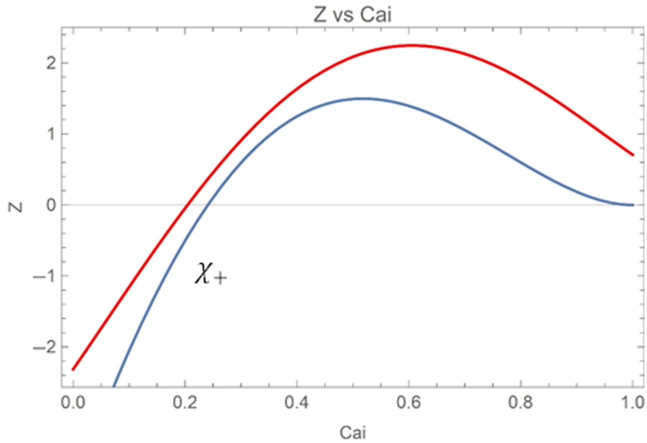

Figure 7. ***Z*** as a function of χ

$$t_{int}{}' = \left(\frac{1}{2}\cdot\frac{N'}{S}\right)$$

N' and S can be expressed as:

$$N' = -2\cdot(1-\chi)\cdot\left(1-\chi\cdot\tan^2(\theta)+2\cdot\chi^2\cdot\tan^2(\theta)\right)$$

$$S = 2\cdot\alpha\cdot\gamma - N'$$

Thus, $N' = 2\cdot\alpha\cdot\gamma - 2\cdot S$. Hence, as the interceptor reaches its detonation range to the RV $(\chi \to 1)$:

$$T' = 1 + \left(\frac{1}{2}\cdot\frac{2\cdot\alpha\cdot\gamma - 2\cdot S}{S}\right) = \frac{\alpha\cdot\gamma}{S} > 0 \tag{17}$$

Thus, total intercept time T is increasing at $\chi \to 1$. This proves the existence of the anomaly.

It is very simple to repeat the analysis when $D = 0$. The results on T' still hold when $D = 0$. For example, since $t_{int} = \frac{1}{2}\cdot\frac{N}{S}$, $N \geq 0$ and $Z = S$ then

$$\underset{Z\to 0^+}{lim}\, T = \lim_{Z\to 0^+} t_{int} = \underset{S\to 0^+}{lim}\, t_{int} \to \infty$$

This requires T to be decreasing on the left-hand side.

Uniqueness of the minimal intercept time

Given that the RV's speed is initially greater than the interceptor's speed: $\gamma^2 < 1 + tan^2(\theta)$, we know that $D(0) < 0$. There are two cases to consider:

(1) D can be zero $(\gamma \geq 1)$

(2) $D < 0$ $(\gamma < 1)$

In Case 1, the RV's speed is initially greater than the interceptor's speed, but later, due to gravity, the RV's speed can be equal to the interceptor's speed. In Case 2, the RV's speed is always greater than the interceptor's speed. We will provide the proof for Case 1 below and infer the proof for Case 2 from that of Case 1.

Case 1. $\boldsymbol{D}$ can be zero ($\boldsymbol{\gamma \geq 1}$)

In order to provide tactics to ballistic missile defence operators, it is important to know exactly where the minimal intercept time occurs and whether there is more than one minimum. We will show that the intercept time is a convex function in χ. This means that there is only one minimum. Before providing the proof, we will sketch out the essential ideas. We recall that $T = \chi + t_{int}(\chi)$ and so $T'' = t_{int}'' \geq 0$. We will show that $t_{int}'' \geq 0$ by a new technique. We will illustrate the technique with an example.

Observation 1. Note that $-S + \sqrt{S^2 + D \cdot N} = 0$ only if $D = 0$ and $S \geq 0$ knowing $N > 0$. Both D and N are polynomials in χ. So, in general: $-S + \sqrt{S^2 + D \cdot N} = S \cdot \left(\frac{1}{2} \cdot \left(\frac{D \cdot N}{S^2}\right) + \ldots\right) \neq 0$. We insist that not only $\sqrt{S^2 + D \cdot N} \neq S$, $S < \sqrt{S^2 + D \cdot N}$ if $D \cdot N > 0$ and $S > \sqrt{S^2 + D \cdot N}$ if $D \cdot N < 0$. In essence, they are never equal unless $D \cdot N = 0$. In addition, $D \cdot N$ is a polynomial of degree 6 whose roots do not overlap with those of S^2 for $\alpha > 0$. And so $(\sqrt{S^2 + D \cdot N})'$ is never equal to S', etc. For example, at $D = 0$, $(\sqrt{S^2 + D \cdot N})' = S' + \frac{D' \cdot N}{2 \cdot S}$ where $\frac{D' \cdot N}{2 \cdot S} \neq 0$ since $N > 0$ while D' and S do not have the same roots as those of D. We can also infer that $(\sqrt{S^2 + D \cdot N})'' \neq S''$ at $D = 0$. Assuming the contrary will lead to a contradiction. That is, assuming $(\sqrt{S^2 + D \cdot N})'' = S''$ will make $(\sqrt{S^2 + D \cdot N})' = S'$ at $D = 0$.

But we have shown that $(\sqrt{S^2 + D \cdot N})' = S' + \frac{D' \cdot N}{2 \cdot S}$ with $\frac{D' \cdot N}{2 \cdot S} \neq 0$. Therefore, this is a contradiction.

Observation 2. $t'_{int} = \left(\frac{-S + \sqrt{S^2 + D \cdot N}}{D}\right)'$. In general, $t'_{int} \neq 0$ except possibly at $D = 0$ because if $t'_{int} = 0$ then $\left(\frac{\sqrt{S^2 + D \cdot N}}{D}\right)' = \left(\frac{S}{D}\right)'$ which is impossible for $D \neq 0$ and $N > 0$. Calculus dictates that:

$$t'_{int} \cdot D^2 = \left(-S + \sqrt{S^2 + D \cdot N}\right)' \cdot D - D' \cdot \left(-S + \sqrt{S^2 + D \cdot N}\right) = FSign \tag{18}$$

when $D = 0$, $FSign = 0$ is zero. The derivative $FSign$ is also zero when $D = 0$:

$$FSign' = \left(-S + \sqrt{S^2 + D \cdot N}\right)'' \cdot D - D'' \cdot \left(-S + \sqrt{S^2 + D \cdot N}\right)$$

However, the second derivative of $FSign$ is not zero at $D = 0$. This holds because

$FSign''\rbrack_{D=0} = A/B\rbrack_{D=0}$ where B is a power of $S\rbrack_{D=0}$ which is not zero (Observation 1) and A is a polynomial in χ that does not divide $D(\chi)$ evenly. By the fundamental theorem of algebra, $A\rbrack_{D=0} \neq 0$ as A and D do not have overlapping roots. We have also confirmed this graphically. There are two roots in χ when $D = 0$. This means that each of these roots are double roots and so $t'_{int} \cdot D^2$ is either non-negative or non-positive. What is more, these are all the roots as

$FSign = FSign' = 0$ only when $D = 0$ (for D real & χ real and in the feasible range). To do that, we determine $t'_{int} \cdot D^2$ at a feasible χ (at $\chi \to 1^-$) and show that $t'_{int} \cdot D^2 < 0$ for that χ. That is sufficient to show that $t'_{int} \cdot D^2 < 0$ for all feasible χ. We plot $FSign = t'_{int} \cdot D^2$ as a function of χ in Figure 8 to illustrate this is the case.

From Equation (17), we get:

$$\lim_{\chi \to 1^-} t'_{int} = \frac{\alpha \cdot \gamma - S}{S} < 0$$

as $\lim_{\chi \to 1^-} S > \alpha \cdot \gamma$.

Since $t'_{int} \cdot D^2 \leq 0$ and $D^2 \geq 0$, then $t'_{int} \leq 0$. In the same way, we can show that $t''_{int} \cdot D^2 \geq 0$. Therefore, $t''_{int} \geq 0$. Since $T = \chi + t_{int}$, we know $T'' = t_{int}{}'' \geq 0$. This completes the proof of convexity. Knowing there is exactly one minimum lying between zero and one, we determine the value of $\chi = \chi_{min}$ using bisection (Wikipedia, n.d.a, n.d.b, accessed 2024). This guarantees a solution to the desired accuracy.

Observation 3. We sketch below the proof of convexity. (Quotient rule 2024) gives:

$$t''_{int} \cdot D^2 = \left(Z'' - D'' \cdot t_{int} - 2 \cdot D' \cdot t'_{int}\right) \cdot D \tag{19}$$

We will show that

$$\left(Z'' - D'' \cdot t_{int} - 2 \cdot D' \cdot t'_{int}\right)\Big]_{D=0} = 0 \tag{20}$$

This means that the right-hand side of Equation (19) has at least a double root at $D = 0$. Simple calculus yields:

$$Z''\Big]_{D=0} = \frac{-D'^2 \cdot N^2 + 2 \cdot D'' \cdot N \cdot S^2 + 4 \cdot D' \cdot N' \cdot S^2 - 4 \cdot D' \cdot N \cdot S \cdot S'}{4 \cdot S^3} \tag{21}$$

Differentiating Equation (11) and letting $D = 0$, we get:

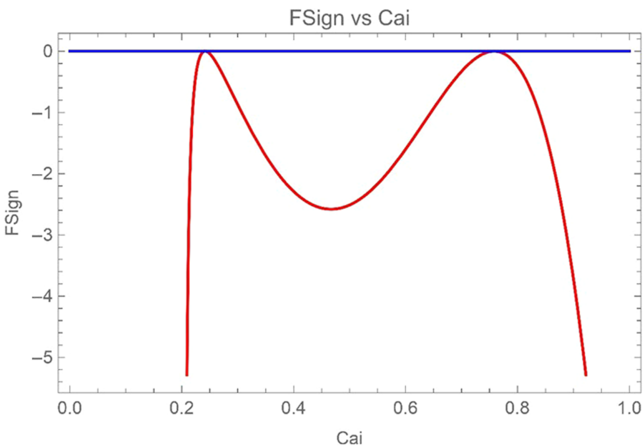

Figure 8. ***FSign*** **as a function of χ with $\gamma = 1.682$, *tan* $\theta = -2.619$ and $\alpha = 0.3$**

$$2 \cdot S \cdot T' = N' - D' \cdot \left(\frac{N}{2 \cdot S}\right)^2 - 2 \cdot S' \cdot \left(\frac{N}{2 \cdot S}\right) \tag{22}$$

Where $\left.t_{int}\right]_{D=0} = \frac{1}{2} \cdot \frac{N}{S}$. Using Equations (12), (21) and (22), we establish Equation (20). Furthermore, we can verify that

$$\left.\left(Z'' - D'' \cdot t_{int} - 2 \cdot D' \cdot t'_{int}\right)'\right]_{D=0} \neq 0$$

Using the same argument as the one used in Observation 2. Since the right-hand side of Equation (19) is the product of Equation (20) and D, this implies that Equation (19) has a double root at $D = 0$. In addition, D is a quadratic function in χ so each root of D is a double root as seen in Figure 9. We plot Equation (20) and D as a function of χ in Figure 10. The blue curve corresponds to D and the red curve corresponds to Equation (20). They clearly have the same roots.

We now show that $\lim_{\chi \to 1^-} t''_{int} > 0$. Note that we can obtain $\lim_{\chi \to 1^-} t''_{int}$ by differentiating Equation (11) twice and setting:

$$N = 0$$

$$t_{int} = 0$$

$$2 \cdot S = 2 \cdot \alpha \cdot \gamma - N'$$

Also, when $\chi \to 1^-$:

$$S > \alpha \cdot \gamma$$

$$S' \to -\left(1 + tan^2\, \theta\right)$$

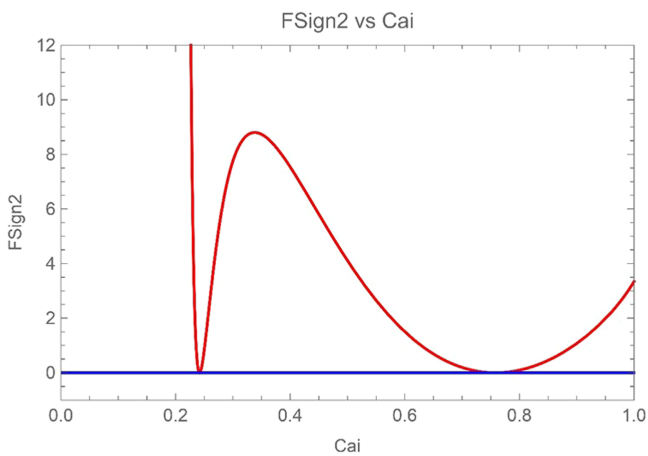

Figure 9. $\boldsymbol{FSign2 = t''_{int} \cdot D^2}$ as a function of χ with $\boldsymbol{\gamma = 1.682}$, $\boldsymbol{tan\,\theta = -2.619}$ and $\boldsymbol{\alpha = 0.3}$

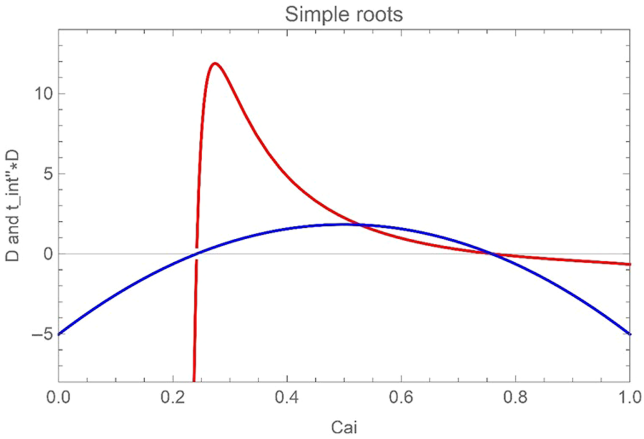

Figure 10. $\boldsymbol{FSign2/D = t''_{int} \cdot D}$ **and** $\boldsymbol{D}$ **as a function of** $\boldsymbol{\chi}$ **with** $\boldsymbol{\gamma = 1.682}$**,** $\boldsymbol{tan\,\theta = -2.619}$ **and** $\boldsymbol{\alpha = 0.3}$

$$t'_{int} \to \frac{\alpha \cdot \gamma - S}{S}$$

$$D \to \gamma + S'$$

This yields:

$$S \cdot T'' = -S' \cdot \left(1 + t'_{int}\right)^2 - \gamma \cdot \left(t'_{int}\right)^2$$

$$S \cdot T'' \to \frac{1}{cos^2\,\theta} \cdot \left(1 - \frac{v^2}{u^2}\right) \Big\rangle 0$$

Case 2. $\boldsymbol{D < 0\ (\gamma < 1)}$

In essence, we show in Case 1 that $FSign2$ has the same roots as $D(\chi)$. So, if $D(\chi) < 0$ then D has no real roots and so $FSign2$ also has no real roots (in the feasible range). This means that $FSign2$ is either positive or negative but not both. In addition, Equation (18) tells us that T'' has the same sign as $FSign2$, and we show above that $T'' > 0$ for $\chi \to 1^-$. This concludes that $T'' > 0$, in the feasible range. An illustration of $FSign2$ is shown in Figure 11 where $\gamma = 0.8 < 1$.

Examples

To validate the results derived in the previous sections, we compare them to those of MANA (Map-Aware Non-uniform Automata), which is an agent-based model developed by the Defence Technology Agency of New Zealand (Lauren and Stephen, 2002). Agent-based simulations and characteristics abound and their descriptions can be found, for example, in Castle and Crooks (2006) and Diallo *et al.* (2015). Our results (dashed line) and those from MANA (bold line) are consistent, as shown in Figure 12.

To understand the results, we analyse the intercept time with a range of 200 km (solid yellow curve) shown in Figure 12. In Case 1, if the defence waits for 50 s after the RV is launched, the intercept occurs at approximately 300 s. In *Case 2*, if the defence waits for 100 s

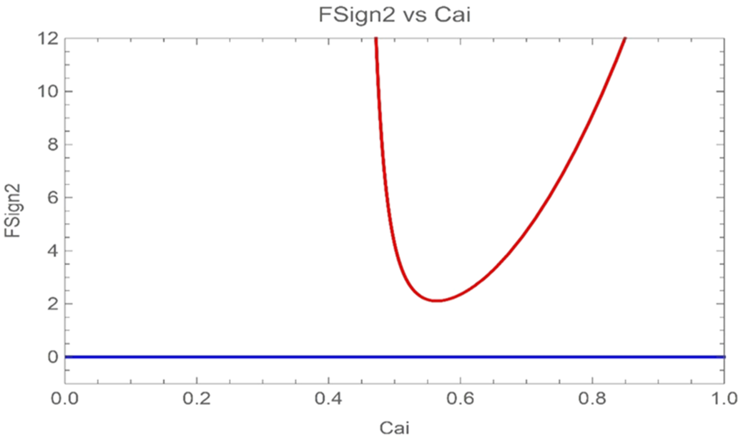

Figure 11. $\boldsymbol{FSign2 = t''_{int} \cdot D^2}$ as a function of $\boldsymbol{\chi}$ with $\boldsymbol{\gamma = 0.8}$, $\boldsymbol{\tan\theta = -2.619}$ and $\boldsymbol{\alpha = 0.3}$. Note that we have assumed that $S]_{D=0} > 0$. It can happen that $S]_{D=0} < 0$ for one root in χ and that $S]_{D=0} > 0$ for the other root in χ in which case $FSign2 = 0$ only for $S]_{D=0} > 0$. The results still hold. If $S]_{D=0} < 0$ for both roots, then $FSign2 < 0$ in the feasible range of χ. Again, the results will hold

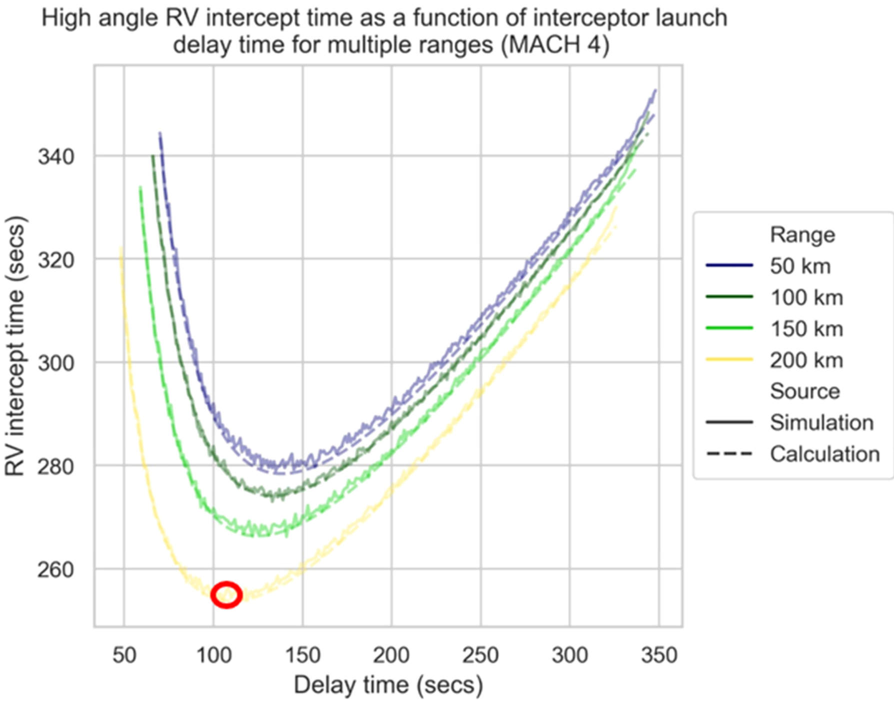

Figure 12. RV (lofted trajectories) intercept time as a function of interceptor launch delay time for multiple ranges obtained from MANA (bold line) and calculation (dashed line) (interceptor speed MACH 4)

after the RV is launched, the intercept occurs at approximately 250 s. This includes the 100 s delay. That is, the RV is launched at time zero, the interceptor is launched at time 100 s and the intercept occurs at time 250 s. This means that the time of flight of the interceptor is 150 s ($250 - 100 = 150$ s). At this interceptor launch delay time, we note that the RV intercept time is also a minimum. With an interceptor launch delay time equal to 50 s (100 s) the RV intercept time is equal to 300 s (250 s). The time line for Case 1 and Case 2 are shown in Figure 13.

There are many advantages to intercepting the RV at optimal delay. First, the time of flight of the interceptor is shorter, which increases the reliability of the operation of the interceptor. Second, an early intercept generally means the RV is intercepted further from the target, which reduces the secondary effects of debris. Third, having more time is always a benefit. In this example, a saving of 100 *secs* out of 350 *secs* is 28 *percent*, which is substantial in time-critical intercepts.

Figure 14 shows the straight-line solutions: the RV trajectory is affected by gravity until the launch of the interceptor. After the launch of the interceptor, both vehicles move in straight lines in the solution space since the gravitational acceleration terms cancel. Figure 15 shows the actual physical solutions: both vehicles are subjected to gravity even after the launch of the interceptor. That is, gravitational acceleration is added back to both trajectories even though the gravitational terms cancel mathematically after the launch of the interceptor. In the solution space, Figure 14 shows that the intercept occurs at a higher altitude than that of Figure 15. This holds as gravity pulls both vehicles towards the ground. The intercept time is, however, unchanged.

The intercept time formula allows examination of the detonation range. The detonation range of Patriots is in the order of meters, which is much less than the range of RV (in the order of kilometres). In the future, it is possible that interceptors will have greater detonation ranges. Figure 16 shows the non-linearity of the intercept time when the speed ratio β decreases (slow interceptors) and the detonation range increases. This happens because the detonation range becomes more important when the interceptor is slower. As β increases, the intercept time becomes more linear, as shown by the straight contours. Eventually, when $\beta > 1$ there is no anomaly.

Discussion and conclusion

In this article, we have shown that there is an anomaly in intercept time: the wisdom of launching the interceptor as early as possible does not apply here. There is an optimal launch delay which results in a saving of 28 *percent* in time in the scenario considered. We show exactly when and why the anomaly occurs. This happens when the interceptor's speed is less than the RV's speed and the RV travels in a lofted trajectory. As described, there are actual RVs,

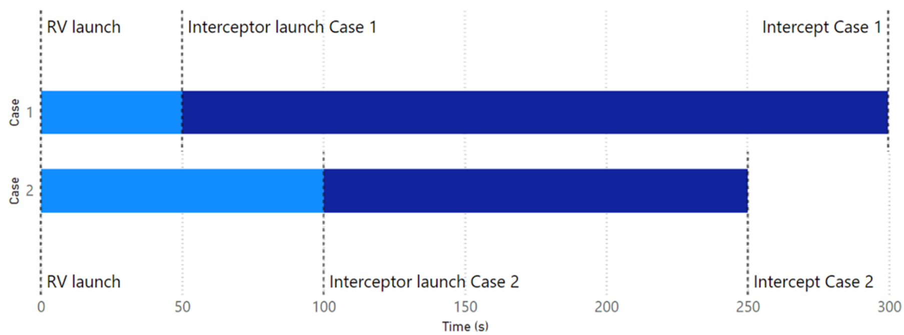

Figure 13. An example of intercept timeline

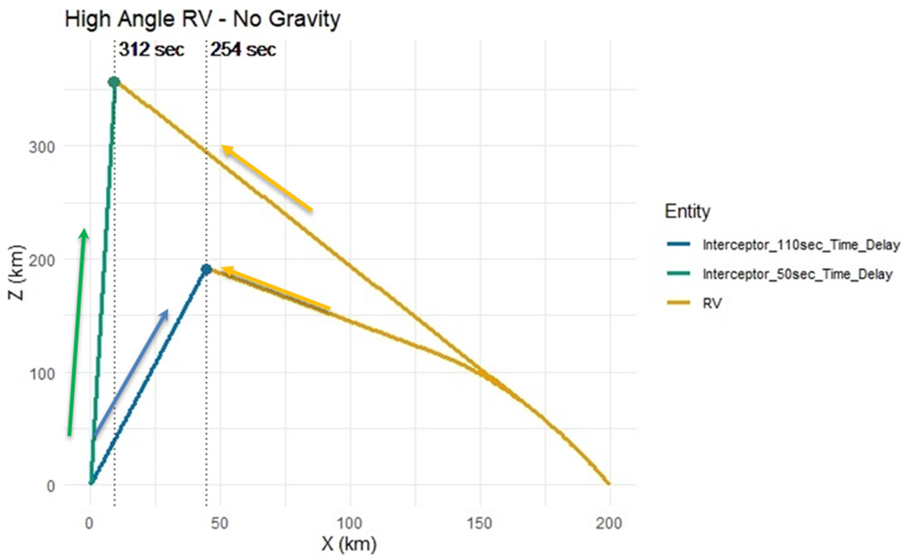

Figure 14. Feasible straight-line intercept for two interceptor launch delay times without gravity after interceptor launching. Interceptor speed is MACH 4 from left to right and RV speed is MACH 5 from right to left

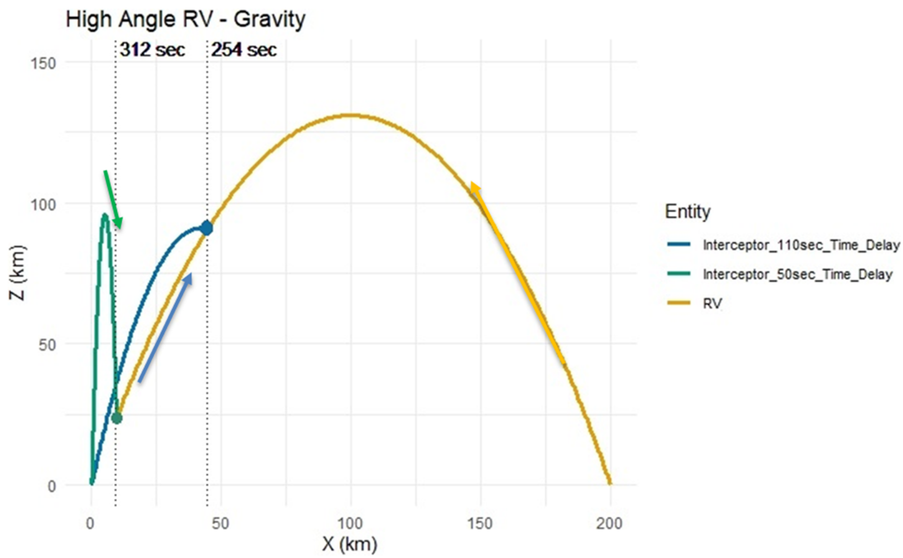

Figure 15. Feasible ballistic trajectory intercept for two interceptor launch delay times with gravity. Interceptor speed is MACH 4 from left to right and RV speed is MACH 5 from right to left

such as North Korean Hwasong 17 and Hwasong 18 missiles, which travel in lofted trajectories, and they are harder to detect. Hence, it is an advantage to the offense. With hypersonic RVs, it will also not be surprising that the defence needs to intercept a faster RV. A non-zero detonation range becomes a key parameter in such a scenario as it raises the capabilities of the interceptor, especially against a fast RV. In fact, there have been cases in

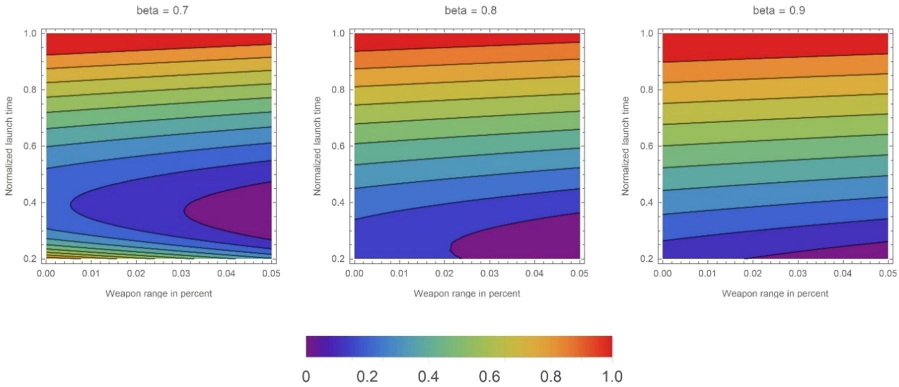

Figure 16. Contour plot of intercept time as a function of speed ratio and detonation range

Ukraine where the Patriot defence system has intercepted a hypersonic RV (the hypersonic speed was greater than the Patriot's speed).

From a methodological viewpoint, we have developed simple tools to analyse a complex and non-linear problem. Without these tools, it would not have been possible to derive the intercept time formula. The formula provides insights into the convexity of the problem, yielding a unique optimal launch time. It tells us when and why the anomaly occurs. The formula also yields the concept of a feasible volume of approach. That is, based on the initial conditions, such as locations and velocities, it may not be feasible at all to intercept an RV. The defence would need to wait for the RV to change its velocity vector before an intercept is possible. Hence, there is an optimal launch delay which can be determined with the desired accuracy in an efficient way. In a two-dimensional maritime context, the feasible volume of approach is known as the limiting lines of approach. The time intercept formula quantifies the effects on the detonation range, both on the intercept time and the feasible volume of approach. That is, the intercept occurs earlier, and the feasible volume of approach gets larger with a non-zero detonation range. If we had simplified the trajectories as straight lines, then the anomaly would not have been discovered and the intercept time would have had the wrong pattern: a monotonically increasing function as opposed to a convex function in launch delay time. In general, we believe that convexity can be exploited in many other defence and optimization problems.

References

Ann, S., Lee, S., Kim, Y. and Ahn, J. (2020), "Midcourse guidance for exoatmospheric interception using response surface based trajectory shaping", *IEEE Transactions on Aerospace and Electronic Systems*, Vol. 56 No. 5, pp. 3655-3673, doi: 10.1109/taes.2020.2976084.

Armstrong, M.J. (2014), "Modeling short-range ballistic missile defense and Israel's Iron Dome system", *INFORMS*, Vol. 62 No. 5, pp. 1028-1039, doi: 10.1287/opre.2014.1309.

Bate, R.R., Mueller, D.D. and White, J.E. (1971), *Fundamentals of Astrodynamics*, Dover Publications, New York.

Bourn, S. (2012), "Probabilistic shoot–look–shoot combat models", PhD thesis, School of Mathematical Sciences, The University of Adelaide, Adelaide, Australia, available at: https://digital.library.adelaide.edu.au/dspace/handle/2440/73043 (accessed January 2022).

Buontempo, J.T. (2015), "A trajectory for homeland ballistic missile defense", *Defense and Security Analysis*, Vol. 31 No. 2, pp. 99-109, doi: 10.1080/14751798.2015.1014157.

Carnegie Endowment for International Peace (2021), “Carnegie endowment for international Peace, reports, ballistic missile defenses”, pp. 73-78, 2021.

Carpentier, G.J.P.de (2014), “Analytical ballistic trajectories with approximately linear drag”, *International Journal of Computer Games Technology*, Vol. 2014, pp. 1-13, 2014 doi: 10.1155/2014/463489.

Castle, C.J.E. and Crooks, A.T. (2006), *Principles and Concepts of Agent – Based Modelling for Developing Geospatial Simulations*, Centre for Advanced Spatial Analysis – London University College.

Cranford, K. (2004), “Battle area region threatened model (BART)”, *NORAD – USNORTHCOM/AN (North American Aerospace Defense Command – United States Northern Command/Center for Aerospace Analysis)*, version 5.3.4x (accessed January 2014).

Diallo, S.Y., Lynch, C.J., Gore, R. and Padilla, J.J. (2015), “Emergent behavior identification within an agent – based model of the ballistic missile defense system using statistical debugging”, *Journal of Defense Modeling and Simulation*, Vol. 13 No. 3, pp. 275-289, doi: 10.1177/1548512915621973.

Glover, L.S. and Hagan, J.C. (1971), “The motion of ballistic missiles”, in *Applied Physics Laboratory – Technical Memorandum*, The Johns Hopkins University, MD, available at: https://apps.dtic.mil/sti/tr/pdf/AD0731662.pdf (accessed April 2024).

Lauren, M.K. and Stephen, R.T. (2002), “Map-aware non-uniform automata (MANA) – a New Zealand approach to scenario modelling”, *Journal of Battlefield Technology*, Vol. 5 No. 1, pp. 27-31.

Lendon, B. and Bae, G. (2023), *North Korea Test Fires Ballistic Missile with Potential to Reach Entire US, Japan Says*, CNN, available at: https://www.cnn.com/2023/12/18/asia/north-korea-launches-ballistic-missile-intl-hnk-ml/index.html (accessed April 2024).

Lui, D., Tartaglione, G., Conti, F., Tommasi, G.D. and Santini, S. (2023), “Long short-term memory-based neural networks for missile maneuvers trajectories prediction”, *IEEE Access*, Vol. 11, pp. 30819-30831, doi: 10.1109/access.2023.3262023.

Menq, J., Tuan, P. and Liu, T. (2007), “Discrete Markov ballistic missile defense system modeling”, *European Journal of Operational Research*, Vol. 178 No. 2, pp. 560-578, doi: 10.1016/j.ejor.2005.12.043.

Mury, B. and Nguyen, B. (2007), “A recursive engagement simulation tree (REST) for use in maritime defence”, DRDC Atlantic TM 2006-096.

Nguyen, B.U. (2014), “Assessment of a ballistic missile defense system”, *Defense and Security Analysis*, Vol. 30 No. 1, pp. 4-6, doi: 10.1080/14751798.2013.864870.

Nguyen, B. and Nguyen, D. (1996), “Optimal intercept course of vessels to a non–zero range”, *SIAM Review*, Vol. 38 No. 4, pp. 647-649, doi: 10.1137/S0036144594286500.

Nguyen, B., Smith, P.A. and Nguyen, D. (1997), “An engagement model to optimize defence against a multiple attack assuming perfect kill assessment”, *Naval Research Logistics*, Vol. 44 No. 7, pp. 687-697, doi: 10.1002/(sici)1520-6750(199710)44:7<687::aid-nav6>3.3.co;2-v.

Nguyen, B.U., Amyot-Bourgeois, M. and Astles, B.C. (2022), “An anomaly in intercept time for short range ballistic re-entry vehicles”, *Proceedings of the 2022 Winter Simulation Conference*, pp. 2025-2033.

Pleitgen, F. (2024), *CNN Gets a Rare Look at the Iranian Missiles and Drones that Hit Israel*, CNN, available at: https://www.cnn.com/2024/05/01/middleeast/iranian-missiles-drones-that-hit-israel-mime-intl/index.html (accessed May 2024).

Soland, R.M. (1987), “Optimal terminal defense tactics when several sequential engagements are possible”, *Operations Research*, Vol. 35 No. 4, pp. 537-542, available at: https://doi.org/10.1287/opre.35.4.537 (accessed January 2022).

Spender, T. (2024), “What was in wave of Iranian attacks and how were they thwarted?”, *BBC News*, available at: https://www.bbc.com/news/world-middle-east-68811273 (accessed May 2024).

Vallado, D.A. (1997), *Fundamentals of Astrodynamics and Applications*, McGraw–Hill Primis Custom Pub, Howthorne, CA.

Weitz, R. (2013), "US missile defense: closing the gap", *World Affairs*, Vol. 176 No. 2, pp. 80-87, available at: https://www.jstor.org/stable/43554784 (accessed January 2022).

Wikipedia (2022a), *MIM-104 Patriot*, Wikipedia, available at: https://en.wikipedia.org/wiki/MIM-104_Patriot (accessed January 2022).

Wikipedia (2022b), *Scud Missile*, Wikipedia, available at: https://en.wikipedia.org/wiki/Scud_missile (accessed January 2022).

Wikipedia (n.d.a), *Bisection Method*, Wikipedia, available at: https://en.wikipedia.org/wiki/Bisection_method (accessed August 2024).

Wikipedia (n.d.b), *Quotient Rule*, Wikipedia, available at: https://en.wikipedia.ord/wiki/Quotient_rule (accessed August 2024).

Wilkening, D.A. (1999), "A simple model for calculating ballistic missile defense effectiveness", *Science and Global Security*, Vol. 8 No. 2, pp. 183-215, doi: 10.1080/08929880008426475.

Further reading

Parametric Technology Corporation (2007), "Mathcad 14.0", available at: https://www.ptc.com

Wolfram Research, Inc (2020), "Mathematica", Champaign, IL, Version 12.2, available at: https://www.wolfram.com

Corresponding author
Phuc Bao Uyen Nguyen can be contacted at: p.bao.u.nguyen@gmail.com